Int. J. Electrochem. Sci., 7 **(2012)** 3982 - 3996

International Journal of
ELECTROCHEMICAL
SCIENCE
www.electrochemsci.org

Investigation of Newly Pyridazine Derivatives as Corrosion Inhibitors in Molar hydrochloric Acid. Part III: Computational Calculations

Z. El Adnani[1,2], *M. Mcharfi*[1], *M. Sfaira*[2,*], *A.T. Benjelloun*[1], *M. benzakour*[1], *M. Ebn Touhami*[3], *B. Hammouti*[4], *M. Taleb*[2]

[1] Equipe de Chimie Informatique et Modélisation, Laboratoire d'Ingénierie des Matériaux, Modélisation et Environnement, LIMME, Faculté des Sciences Dhar El Mahraz, Université Sidi Mohammed Ben Abdellah, BP 1796 – 30000, Atlas – Fès, Morocco.
[2] Equipe de Matériaux et Traitement de Surfaces, Laboratoire d'Ingénierie des Matériaux, Modélisation et Environnement, LIMME, Faculté des Sciences Dhar El Mahraz, Université Sidi Mohammed Ben Abdellah, BP 1796 – 30000, Atlas – Fès, Morocco.
[3] Laboratoire des Matériaux, Electrochimie et Environnement, Faculté des Sciences, Université Ibn Tofaîl, BP. 133 – 14000, Kénitra, Morocco.
[4] LCAE-URAC18, Faculté des Sciences, Université Mohammed Premier, BP 717 – 60000, Oujda, Morocco.
[*] E-mail: msfaira@yahoo.com

Received: 21 March 2012 / *Accepted:* 7 April 2012 / *Published:* 1 May 2012

Quantum chemical calculations, based on DFT methods at B3LYP/6-31G** level of theory, were performed, by means of the GAUSSIAN 03 set of programs, on four recognized pyridazine compounds as corrosion inhibitors in acidic media. The objective of this work is to attempt to find relationships between their molecular and electronic structures and inhibition efficiency. The structural parameters, such as the frontier molecular orbital energies (E_{HOMO} and E_{LUMO}), gap of energy ΔE, the charge distribution, the absolute hardness η and softens σ, the fraction of electrons ΔN transferred from pyridazine molecules to iron as well as electronic parameters such as Mulliken atomic populations and Fukui indices were calculated and discussed. The behaviour of these organic molecules in the presence of solvents, among them water, has facilitated the understanding of the corrosion inhibition process. Significant correlations were obtained between the calculated descriptors and experimental outcomes. The study clearly show that the substitution of an oxygen atom by sulphur one was very beneficial towards corrosion inhibition of mild steel in 1 M HCl.

Keywords: Computational chemistry; Pyridazine; Corrosion inhibition; DFT; Descriptors

1. INTRODUCTION

Corrosion of mild steel is an inevitable process that produces a deterioration of materials and their properties resulting in massive economic losses especially when it's occur in aggressive media like hydrochloric acid. Since we cannot stop its happening, the ultimate solution is at least to prolong the life of the metallic structures and components exposed to such environment. The use of organic compounds, as corrosion inhibitors, constitutes one of the most common, effective and economic method to protect metals against corrosion.

The inhibitory effect of an organic inhibitor is reinforced by the presence of heteroatoms such as phosphorus, sulphur, nitrogen and oxygen in its molecule which facilitates its adsorption on the metal surface following the sequence P>S>N>O. Furthermore, former studies concluded that the adsorption on the metal surface depends on the availability of nonbonded lone-pair and π electrons in inhibitor molecules which facilitate electron transfer from the inhibitor to the metal and allow the formation of covalent bond between the inhibitor and the metal surface [1-3]. In addition, some molecular geometry properties of the inhibitors can also play a determined role in the enhancement of their corrosion inhibition efficiencies, such as the planarity of the system, the molecular size and the presence of multiple adsorption active centers with lone pair and/or orbitals whose electronic density is higher at the donor atom. Therefore, the choice of effective inhibitors is usually based on their structure, their mechanism of action and their electron donating ability.

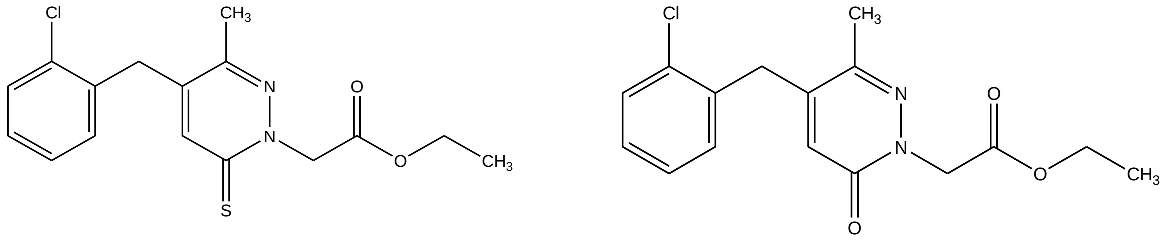

P1: ethyl[4-(2-chlorobenzyl)-3-methyl-6-thioxopyridazin-1(6H)-yl]acetate

P2: ethyl[4-(2-chlorobenzyl)-3-methyl-6-oxopyridazin-1(6H)-yl]acetate

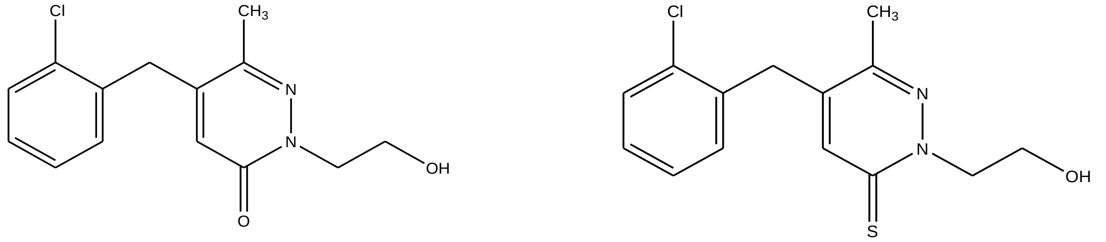

P3: 5-(2-chlorobenzyl)-2-(2-hydroxyethyle)-6-methylpyridazin-3(2H)-one

P4: 5-(2-chlorobenzyl)-2-(2-hydroxyethyle)-6-methylpyridazin-3(2H)-thione

Figure 1. The chemical formulas of the studied pyridazine derivatives

Many N-heterocyclic compounds have been used for the corrosion inhibition of iron or mild steel in acidic media. Their high inhibition efficiencies were attributed to the strong adsorption on the metal surface through their N heteroatom [4-6]. The pyridazine derivatives have been widely reported as good corrosion inhibitors in acidic media [7-10].

The main objective of this work was to investigate computationally, in gas and aqueous phases, using DFT at B3LYP/6-31G** level of theory, four newly synthesized pyridazine derivatives denoted hereafter P1, P2, P3 and P4 as shown in Fig. 1. These inhibitors have been recently reported by B. Zerga et al. [11,12] as novel and effective corrosion inhibitors towards mild steel in hydrochloric acid. The study has been conducted by weight loss measurements and electrochemical (Potentiodynamic polarization and electrochemical impedance spectroscopy EIS) methods. Beside, the inhibiting efficiencies derived from all the studied techniques were in good agreement and followed the same trend as can be seen in Table 1.

Table 1. Experimental inhibition efficiencies of the investigated pyridazine derivatives for steel corrosion in 1 M hydrochloric acid obtained from gravimetric loss, $IE_W\%$, potentiodynamic polarization curves $IE_I\%$ and electrochemical impedance spectroscopy $IE_{imp}\%$ [11,12]

Inhibitor	$IE_W\%$	$IE_{I-E}\%$	$IE_{imp}\%$
P1	100	96	97
P2	92	90	91
P3	89	88	87
P4	92	90	93

In the following, we attempt to find good theoretical parameters to characterize, the inhibition properties of the inhibitors under study and the correlation between the inhibition efficiency and the electronic as well as geometric properties of these molecules.

2. CALCULATION METHODS

The quantum chemical calculations were performed on an Intel (R) core $(TM)_2$ Quad CPU (2.4 GHz and 8 GB RAM) computer using standard Gaussian-03 software package [13] with complete geometry optimizations without constrains.

The geometry optimizations were carried out in gas phase at the Density Functional Theory (DFT) level using the hybrid functional B3LYP based on Becke's three-parameter functional including Hartree–Fock exchange contribution with a nonlocal correction for the exchange potential proposed by Becke [14,15] together with the nonlocal correction for the correlation energy provided by Lee et al. [16]. Indeed, DFT methods are often the methods of choice for similar calculations [15] because of their ability to overcome one of the main disadvantages of ab-initio methods; the complete neglect of electron correlation; by including some of it at greatly reduced computational cost [17]. Thus, all the parameters presented in this work were calculated at B3LYP with 6-31G** basis set, frequently used for similar molecules [18-20].

Since the electrochemical corrosion takes place in the liquid phase; we found relevant to include the effect of solvent in the computations. Self-consistent reaction field (SCRF) theory [15], with Tomasi's polarized continuum model (PCM) [21], was used to perform the calculations in solution at B3LYP/6-31G** level, too. These methods model the solvent as a continuum of uniform dielectric constant (ε) and define the cavity where the solute is placed as a uniform series of interlocking atomic spheres. Since we cannot represent the implicit effect of hydrogen chloride solution, water is instead used to include the solvent effect ($\varepsilon = 78.5$) [22].

The aim of this work is to investigate whether there is a clear relationship between the experimentally determined inhibition efficiencies of the studied inhibitors and a number of quantum-chemical parameters. Some of these parameters are directly extracted from the output files (E_{HOMO}, E_{LUMO}, μ) when other parameters needs to be computed separately (IP, EA, ΔE, χ, η, σ and ΔN).

According to, the Koopmans' theorem [23] for closed-shell molecules, ionization potential IP and electron affinity EA can be expressed as follows in terms of E_{HOMO}, E_{LUMO} the highest occupied molecular orbital energy, and the lowest unoccupied molecular orbital energy, respectively:

$$IP = -E_{HOMO} \tag{1}$$

$$EA = -E_{LUMO} \tag{2}$$

When the values of IP and EA are known, one can determine through the following expressions the values of the absolute electronegativity χ, the absolute hardness η and the softness σ (the inverse of the hardness):

$$\chi = \frac{IP + EA}{2} \tag{3}$$

$$\eta = \frac{IP - EA}{2} \tag{4}$$

$$\sigma = \frac{1}{\eta} \tag{5}$$

Moreover, for a reaction of two systems with different electronegativities the electronic flow will occur from the molecule with the lower electronegativity (the organic inhibitor) towards that of higher value (metallic surface), until the chemical potentials are equal [22]. Therefore the fraction of electrons transferred (ΔN) from the inhibitor molecule to the metallic atom was calculated according to Pearson electronegativity scale [22]:

$$\Delta N = \frac{\chi_{Fe} - \chi_{inh}}{2(\eta_{Fe} + \eta_{inh})} \tag{6}$$

Where χ_{Fe} and χ_{Inh} denote the absolute electronegativity of *Fe* and the inhibitor molecule, respectively; η_{Fe} and η_{inh} denote the absolute hardness of Fe and the inhibitor molecule, respectively. A theoretical value for the electronegativity of bulk iron was used χ_{Fe} = 7 eV and a global hardness of η_{Fe} = 0, by assuming that for a metallic bulk *IP* = *EA* because they are softer than the neutral metallic atoms [23].

Net atomic charges have been obtained using the natural population analysis (*NPA*) of Weinhold [24]. The natural bond orbital analysis allowed us to describe the bonding in terms of the natural hybrids centered on each atom. The population analysis has been performed on the neutral, cationic and anionic species at the same obtained optimized geometry of each inhibitor in order to determine their Fukui Functions.

3. RESULTS AND DISCUSSION

3.1. Molecular geometry

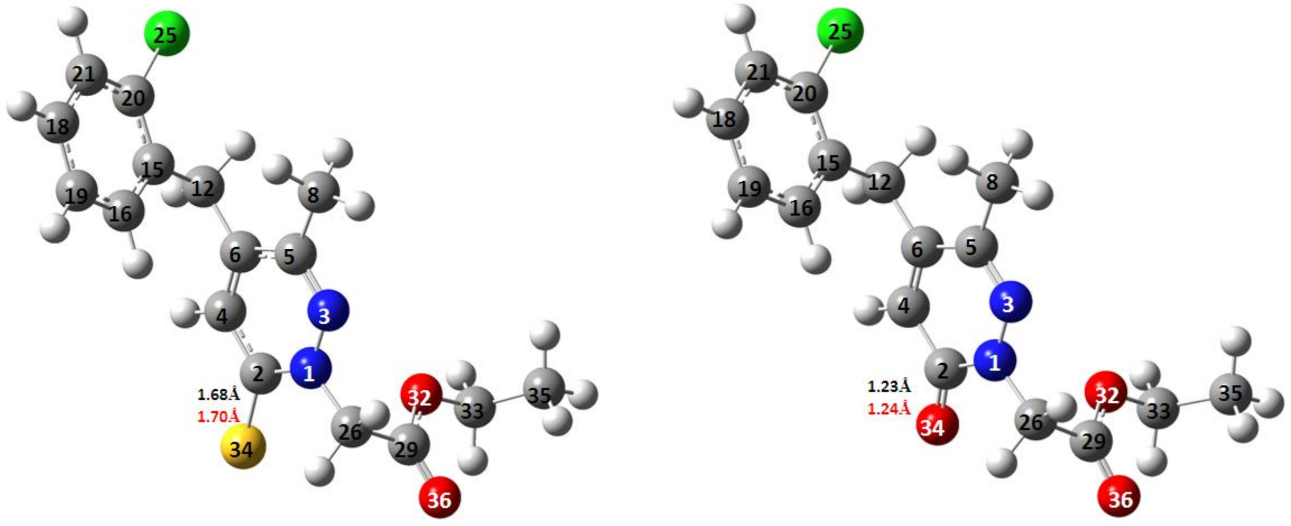

P1 **P2**

Figure 2. Optimized molecular structures of P1 and P2 along with the calculated C2-S34 and C2-O34 bond lengths in gas (black) and aqueous (red) phases

The starting point geometries of the conformational analysis for the four pyridazine derivatives were deduced from a previous conformational study of similar pyridazine derivatives conducted by M. Bouklah et al. [7]. Keeping the backbone structure constant, numerous structures were fully optimized and the minimum of every potential energy surface was qualified by the low energy value and by the absence of imaginary frequencies.

The geometries of all the molecules considered in this work were fully optimized at DFT level of theory using a B3LYP functional together with 6-31 G** basis set in gaseous phase and for a better approach of the experimental parameters, the geometries were re-optimized in aqueous phase at the same level of theory using PCM model. The final geometries are given in Figures 2 and 3.

Table 2. Pertinent dihedral angels of the studied inhibitors calculated at B3LYP/6-31G** in gas, *G* and aqueous, *A* phases

Dihedral angle	Phase	P1	P2	P3	P4
[C6,C12,C15,C16]	G	25°	23°	25°	29°
	A	25°	22°	21°	22°
[N1,C26,C29,O32]	G	14°	17°	54°	51°
		22°	28°	84°	54°
[N3,N1,C26,C29]	G	99°	104°	95°	85°
	A	104°	112°	112°	85°
[C26,C29,O32,C33]	G	180°	180°	-	-
	A	178°	178°		
[C29,O32,C33,C35]	G	86°	86°	-	-
	A	86°	87°		
[C26,C29,O32,H35]	G	-	-	23°	42°
	A			40°	41°

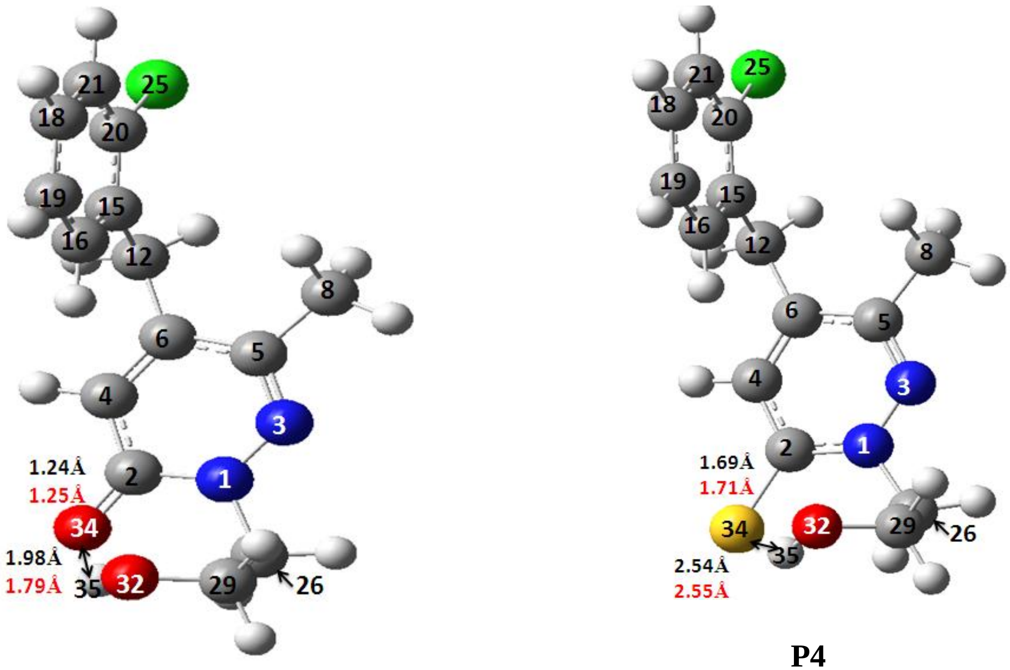

P3 **P4**

Figure 3. Optimized molecular structures of P3 and P4 along with the calculated C2-S34 and C2-O34 bond lengths as well as the intramolecular hydrogen bonding in gas (black) and aqueous (red) phases

Table 2 exemplifies the dihedrals angles derived from the optimized geometry of the studied inhibitors. The geometrical parameters values show no severe difference between gas and aqueous phases for P1, P2 and P4. However, net deviation is registered for the dihedrals [N1,C26,C29,O32], [N3,N1,C26,C29] and [C26,C29,O32,H35] of P3. Indeed, the dihedral value for [N1,C26,C29,O32] goes from 54° in gas phase to 84° in aqueous phase, which can be explained by the enhancement in aqueous phase of the intramolecular hydrogen bonding since the d(O34-H35) vary from 1.98 Å in gas phase to 1.79Å in aqueous phase (Fig. 3). Whereas the d(S34-H35) for P4 remains almost the same; circa 2.54 Å longer than d(O34-H35) in P3.

Moreover, it is shown from the computational results that the substitution of an oxygen atom in P2 and P3 with a sulphur atom in P1 and P4 respectively affect both the molecular and electronic structures of the investigated inhibitors. The substitution leads to a slight increase in the bond lengths. In the case of P2 and P3 the average length of C2-O34 bond is 1.24 Å, Figs. 2 and 3, when the average of the C2-S34 bond in P1 and P4 is 1.70 Å. These results indicate that the adsorption of P1 and P4 on the metal surface through the sulphur atom will be easier and stronger than that through the oxygen atom of P2 and P3 respectively. Indeed, the enhancement of the adsorption is directly related to the increase of the inhibition efficiencies of P1 and P4 with respect to P2 and P3.

3.2. Global molecular reactivity

The chemical reactivity can be explained according to the frontier molecular orbital theory, by the interaction between the HOMO (the highest occupied molecular orbital) and LUMO (lowest unoccupied molecular orbital) of the reacting species. All the global chemical indexes are summarized in Table 3.

Table 3. Quantum chemical descriptors of the studied inhibitors at B3LYP/6-31 G** in gas, *G* and aqueous, *A* phases and the inhibition efficiencies as given in [11,12]

Inhibitor	Phase	E_{HOMO} eV	E_{LUMO} eV	ΔE eV	μ D	EA eV	IP eV	χ eV	η eV	ΔN	IE_{imp} %
P1	*G*	-5.605	-1.986	3.620	5.614	1.986	5.605	3.795	1.809	0.885	97
	A	-6.068	-2.095	3.973	8.399	2.095	6.068	4.081	1.986	0.736	
P2	*G*	-6.286	-1.660	4.636	4.274	1.660	6.286	3.973	2.313	0.654	91
	A	-6.476	-1.714	4.572	5.787	1.714	6.476	4.095	2.381	0.610	
P3	*G*	-6.395	-1.769	4.626	3.476	1.769	6.395	4.082	2.313	0.631	87
	A	-6.558	-1.742	4.816	6.438	1.742	6.558	4.150	2.408	0.592	
P4	*G*	-5.742	-2.041	3.701	4.356	2.041	6.395	4.218	2.177	0.639	93
	A	-6.068	-2.095	3.973	6.550	2.095	6.558	4.326	2.231	0.599	

The E_{HOMO} is often associated with the electron donating ability of the molecules, whereas the E_{LUMO} is associated with the electron accepting ability of the molecules. Therefore, high value of E_{HOMO} indicate high tendency to donate electrons to appropriate acceptor molecule with low empty molecular orbital energy. Likewise, low value of E_{LUMO} indicate high tendency to accept electrons from the metal surface. The obtained values of E_{HOMO} corresponding to each organic inhibitor indicate that the substitution of an oxygen atom in P2 and P3 with a sulphur atom in P1 and P4, respectively increase the E_{HOMO}, which means that the adsorption of P1 and P4 will probably take place through the lone pair of electrons of the sulphur atoms. The results show also that P1 and P4 have the lowest E_{LUMO}

compared to P2 and P3 respectively which indicate a better capability of P1 and P4 to accept electrons and since a good corrosion inhibitor should not only be a good electrons donor but also a good electron acceptor through the back donation mechanism. This result can lead to increase their adsorption on the metal surface and accordingly increases their inhibition efficiency.

The gap between the HOMO and LUMO energy levels of the molecules is another important descriptor that should be considered [25]. Large values of the energy gap (ΔE) imply high electronic stability and then low reactivity, when low values imply that it will be easier to remove an electron from the HOMO orbital to LOMO one which can result in good inhibition efficiency. The results presented in Table 3 show that P1 and P4 containing the sulphur atoms have the lowest energy gapes. Therefore, their higher reactivity can allowed them to be easily adsorbed onto the mild steel surface leading to increase their inhibitive efficiencies compared to P2 and P3, respectively.

Absolute hardness and softness are very important parameters to describe the molecular reactivity and stability. Soft molecules are more reactive than hard ones because they can easily offer electrons. Hence, inhibitors with the highest values of global softness (the least values of the global hardness) are expected to be good corrosion inhibitors for bulk metals in acidic media. The calculations indicate that P1 and P4 have the highest softness values compared to P2 and P3, respectively.

As for the dipole moment, there is an inconsistent in the literature on the correlation between the dipole moment and inhibition efficiency [26,27]. However, it is generally agreed that the adsorption of compounds possessing high dipole moments on the metal surface should lead to better inhibition efficiency [28]. Indeed, the results indicate that P1 and P4 have the highest values of μ compared to P2 and P3, respectively which is in total agreement with the forgoing discussed descriptors.

The fraction of electrons transferred describes the trend of electrons donation within a set of inhibitors. According to Lukovits's study [29], if $\Delta N < 3.6$ then the inhibition efficiency increased with increasing electron-donating ability at the metal surface. The obtained values of ΔN reported in Table 3 are all below 3.6 and P1 and P4 have higher values of ΔN than P2 and P3 respectively. This result implies good disposition of P1 and P4 molecules to donate their electrons leading to increase their adsorption on the metal surface and to increase their inhibition efficiencies.

It is worth noting that all the computed descriptors are in total agreement with the experimental inhibition efficiencies of the four investigated inhibitors, presented in Table 1 which confirm that the substitution of oxygen atoms in P2 and P4 by sulphur atoms in P1 and P4 enhance the donor abilities of these molecules increasing their adsorption on the metal surface and thereby leading to higher experimental inhibition efficiencies. The experimental results also indicate that the substitution of the ethyl ester functional group in C26 position in both P1 and P2 by the methanol group in P4 and P3 respectively reduce the inhibition efficiencies of these inhibitors. The conformational studies of P4 and P3 indicate that the formation of hydrogen bonds probably leads to the stabilization of these inhibitors leading to reduce their respective reactivity. This may explain the decrease of the inhibition efficiencies of P4 and P3 compared to P1 and P2 respectively. Also, the results show that the presence of a sulphur atom in P4 enhance its reactivity despite the presence of the hydrogen bond, since the experimental inhibition efficiency results presented in Table 3 show that P4 presents a better efficiency

(93%) than P2 containing an oxygen atom (91%) which can be explained by the relatively weak engagement of the sulphur atom in the hydrogen bond.

From the computed results in gas and aqueous phases (Table 3), we can easily detect the stabilizing effect of the solvent, since all HOMO energies computed in solution are lower than those computed in gas phase leading to increase their gap energies. Another indicator of this stabilization is the notable decrease in all the four ΔN values.

3.3. Local molecular reactivity

To get some insight into the local reactivity of the studied inhibitors, the Fukui functions were computed since they are the relevant reactivity indicators in the electron-transfer controlled reactions such as corrosion inhibition process [15,30].

Their values are used to identify which atoms in the inhibitors are more prone to undergo an electrophilic or a nucleophelic attack.

For a system of *N* electrons, independent single-point calculations were made for corresponding *N+1* and *N-1* electron systems. The resulting natural population analysis yields to $P_k(N-1)$, $P_k(N)$, and $P_k(N+1)$, the population for all atoms *k*. In a finite-difference approximation from Mulliken population analysis of atoms in molecules, depending on the direction of the electron transfer, then the condensed Fukui functions were computed using the following equations from the Exact Theory [30]:

$$f_k^+ = P_k(N+1) - P_k(N) \qquad \text{(For nucleophilic attack)} \qquad (7)$$

$$f_k^- = P_k(N) - P_k(N-1) \qquad \text{(For electrophilic attack)} \qquad (8)$$

$$f_k^0 = \frac{P_k(N+1) - P_k(N-1)}{2} \qquad \text{(For radical attack)} \qquad (9)$$

The calculated Fukui functions for all the inhibitors are presented in Tables 4 and 5 as well as the corresponding population for the neutral and ionic species. For simplicity, only the highest values of the Fukui functions are presented Tables 4 and 5. It can be noticed that the S34 atoms are the dominant sites susceptible for electrophilic attacks in P1 and P4. These atoms have the highest values of f^- which attain 0.489 in P1 (Fig. 4) and 0.442 in P4 (Fig. 5).

These results can also explain the high corrosion inhibition efficiencies of these molecules when compared with P2 and P3 respectively, where the values of f^- corresponding to the oxygen atoms are only 0.170 in P2 Fig. 4 and 0.163 in P3 (Fig. 5).

Moreover, the distinction of the electron donating abilities between the sulphur and the oxygen atoms became more obvious in the aqueous phase. Indeed, the f^- values of S34 reach 0.705 in P1 (Fig.

4) and 0.751 in P4 (Fig. 5) when the values of f^- corresponding to O34 became 0.244 in P2 (Fig. 4) and 0.249 in P3 (Fig. 4).

On the other hand, most of the atoms in the pyridazine ring (N3, C4 and C6) are susceptible sites for nucleophilic attacks.

These sites present the highest values of f^+ in all the inhibitors. In addition to these sites S34 is also a good site for nucleophilic attacks in P1 and P4 which enhance the adsorption on the metal surface increasing the corrosion inhibition efficiency of these inhibitors.

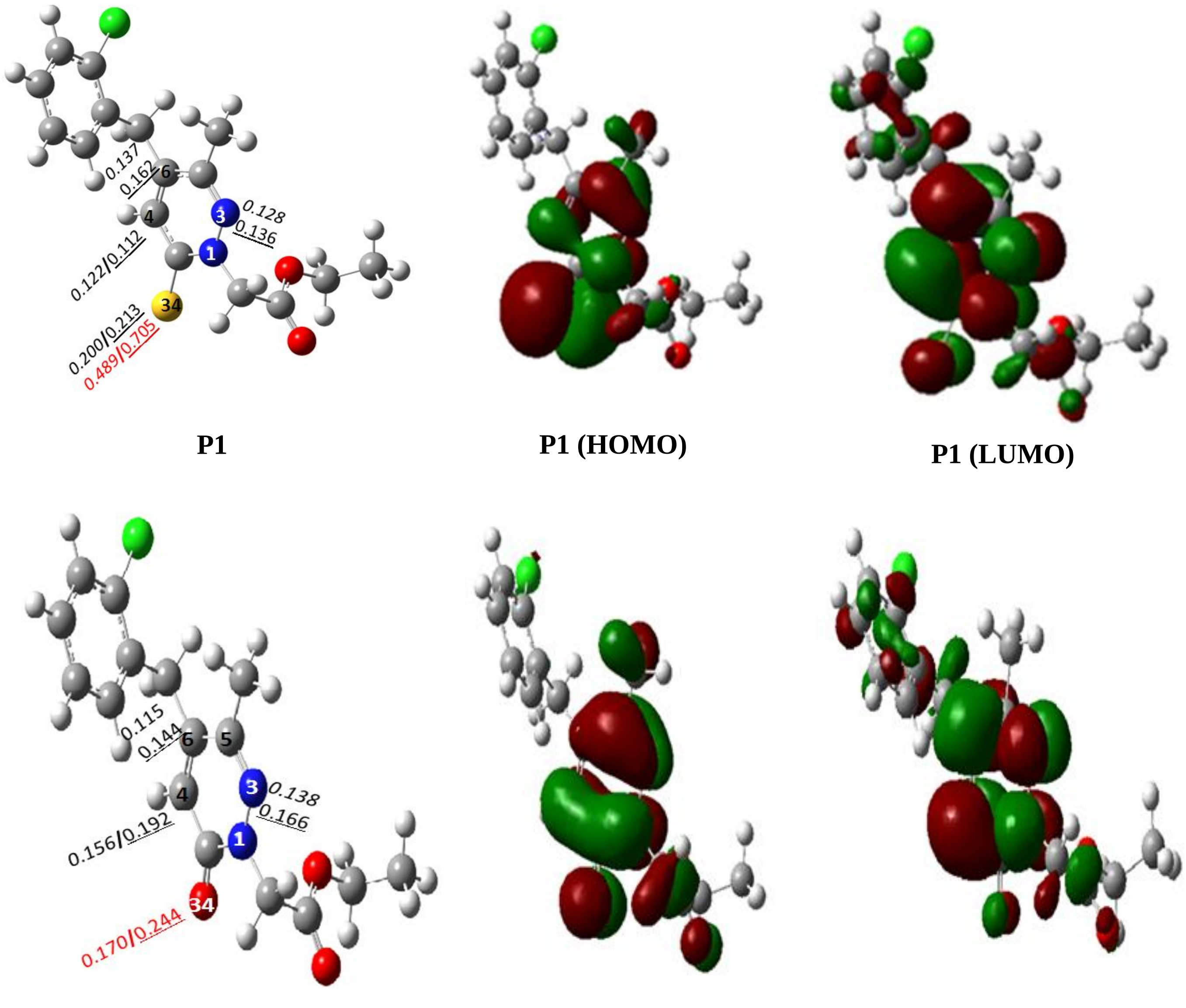

P1 **P1 (HOMO)** **P1 (LUMO)**

P2 **P2 (HOMO)** **P2 (LUMO)**

Figure 4. Fukui functions (f_k^+ black, f_k^- red, *Italic* gas phase, Underline aqueous phase), the Highest Occupied Molecular Orbital HOMO and the Lowest Unoccupied Molecular Orbital LUMO of P1 and P2, computed at B3LYP/6-31G** level in gas phase

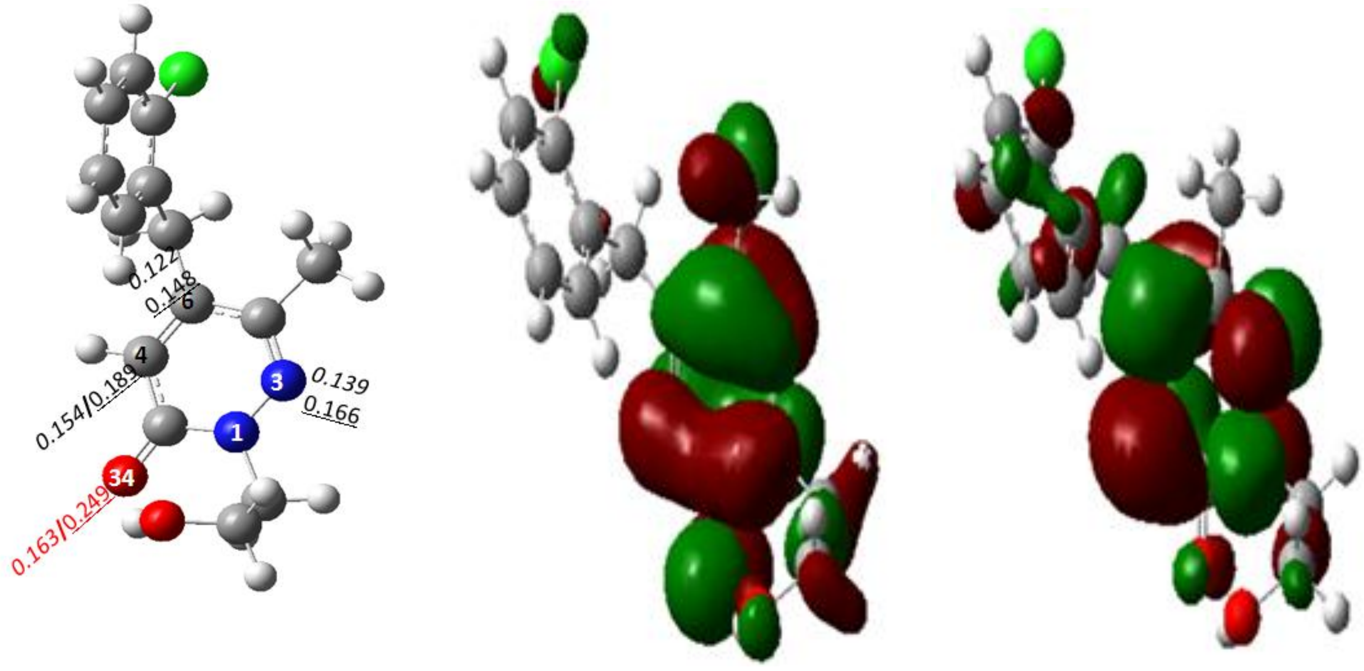

P3 **P3 (HOMO)** **P3 (LUMO)**

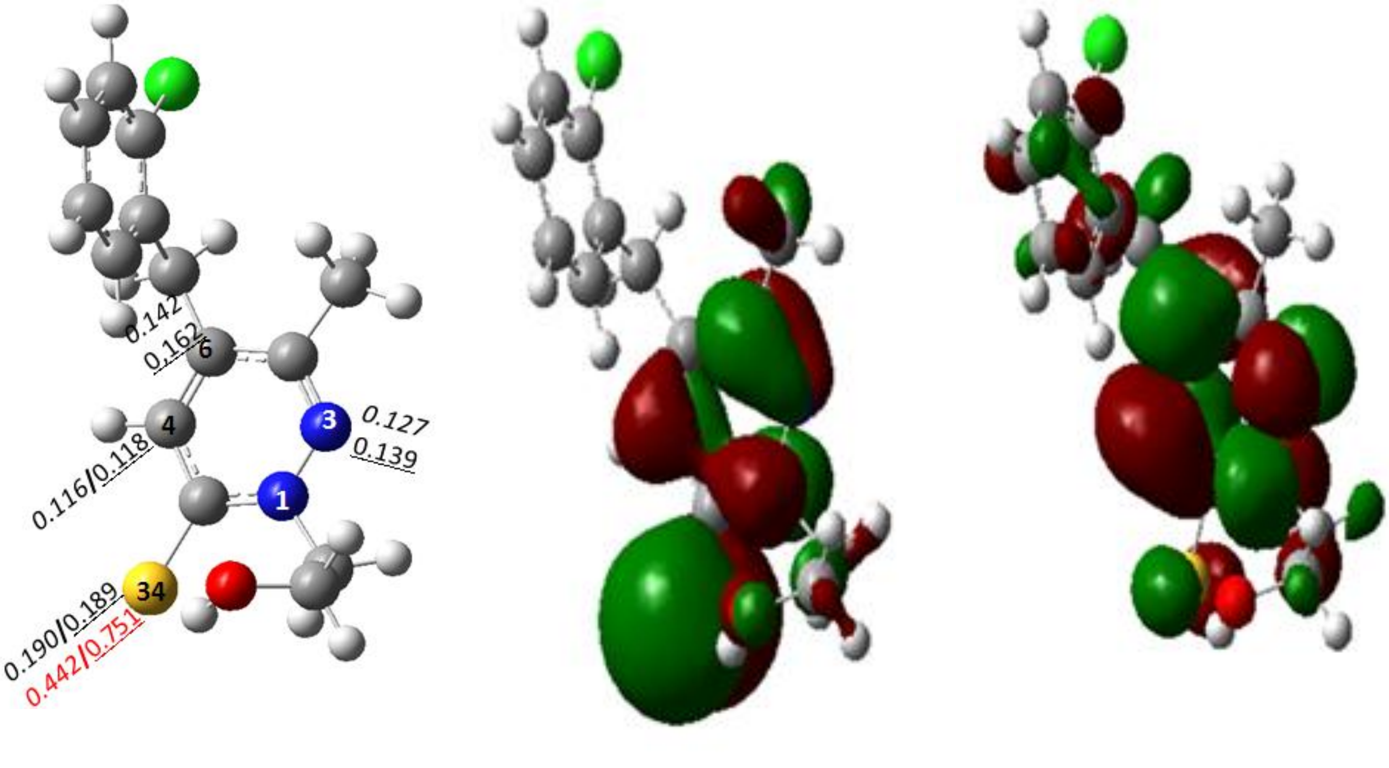

P4 **P4 (HOMO)** **P4 (LUMO)**

Figure 5. Fukui functions (f_k^+ black, f_k^- red, *Italic* gas phase, Underline aqueous phase), the Highest Occupied Molecular Orbital HOMO and the Lowest Unoccupied Molecular Orbital LUMO of P3 and P4, computed at B3LYP/6-31G** level in gas phase

Table 4. Pertinent natural populations and Fukui functions of P1 and calculated at B3LYP/6-31G** in gas, *G* and aqueous, *A* phases

Inhibitor	Atom	Phase	P(N)	P(N+1)	P(N-1)	f_k^+	f_k^-	f_k^0
P1	N1	G	7.174	7.236	7.107	0.062	0.067	0.064
		A	7.159	7.236	7.106	0.077	0.053	0.065
	N3	G	7.231	7.359	7.188	0.128	0.043	0.085
		A	7.238	7.374	7.194	0.136	0.044	0.090
	C4	G	6.204	6.326	6.188	0.122	0.016	0.069
		A	6.209	6.321	6.180	0.112	0.046	0.299
	C5	G	5.787	5.801	5.728	0.014	0.059	0.036
		A	5.768	5.782	5.722	0.014	0.046	0.030
	C6	G	6.032	6.169	5.981	0.137	0.051	0.094
		A	6.005	6.167	5.967	0.162	0.038	0.100
	O32	G	8.551	8.540	8.558	-0.011	-0.007	-0.009
		A	8.548	8.547	8.548	-0.001	0.000	-0.0005
	S34	G	16.188	16.388	15.699	0.200	0.489	0.344
		A	16.329	16.542	15.624	0.213	0.705	0.459
	O36	G	8.597	8.636	8.554	0.039	0.043	0.041
		A	8.632	8.656	8.606	0.024	0.026	0.025
P2	N1	G	7.224	7.283	7.130	0.059	0.094	0.076
		A	7.217	7.287	7.093	0.070	0.124	0.097
	N3	G	7.228	7.366	7.188	0.138	0.04	0.089
		A	7.245	7.411	7.168	0.166	0.077	0.121
	C4	G	6.271	6.427	6.208	0.156	0.063	0.109
		A	6.271	6.463	6.173	0.192	0.098	0.145
	C5	G	5.810	5.837	5.717	0.027	0.093	0.060
		A	5.795	5.836	5.674	0.041	0.121	0.081
	C6	G	6.030	6.145	6.018	0.115	0.012	0.063
		A	6.016	6.160	6.000	0.144	0.016	0.080
	O32	G	8.552	8.540	8.546	-0.012	0.006	-0.003
		A	8.550	8.550	8.545	0	0.005	0.080
	O34	G	8.624	8.703	8.454	0.079	0.17	0.124
		A	8.683	8.768	8.439	0.085	0.244	0.164
	O36	G	8.601	8.640	8.515	0.039	0.086	0.062
		A	8.637	8.661	8.585	0.024	0.052	0.038

The comparison of Fukui functions and the density distribution over the whole skeleton of the molecules presented in Figs. 4 and 5, show high consistency in the local reactivity of these molecules. Since the HOMO is mostly located on the pyridazine ring and on the sulphur atom in the case of P1 and P4, and on the oxygen in the case of P2 and P3. This result also confirms that the adsorption on the metal surface will occur through pyridazine ring and the sulphur atoms.

Table 5. Pertinent natural populations and Fukui functions of P3 and P4 calculated at B3LYP/6-31G** in gas, *G* and aqueous, *A* phases

Inhibitor	Atom	Phase	P(N)	P(N+1)	P(N-1)	f_k^+	f_k^-	f_k^0
P3	N1	G	7.218	7.279	7.136	0.061	0.082	0.071
		A	7.213	7.288	7.084	0.075	0.129	0.102
	N3	G	7.229	7.368	7.190	0.139	0.039	0.089
		A	7.242	7.408	7.167	0.166	0.075	0.120
	C4	G	6.269	6.423	6.213	0.154	0.056	0.105
		A	6.264	6.453	6.166	0.189	0.098	0.143
	C5	G	5.806	5.832	5.726	0.026	0.080	0.053
		A	5.792	5.832	5.663	0.040	0.129	0.084
	C6	G	6.025	6.147	6.014	0.122	0.011	0.066
		A	6.012	6.160	5.995	0.148	0.017	0.082
	O32	G	8.775	8.789	8.701	0.014	0.074	0.044
		A	8.804	8.818	8.758	0.014	0.046	0.030
	O34	G	8.661	8.738	8.498	0.077	0.163	0.120
		A	8.700	8.775	8.451	0.075	0.249	0.162
P4	N1	G	7.166	7.230	7.095	0.064	0.071	0.067
		A	7.156	7.237	7.125	0.081	0.031	0.056
	N3	G	7.233	7.360	7.195	0.127	0.038	0.082
		A	7.240	7.379	7.201	0.139	0.039	0.089
	C4	G	6.206	6.322	6.178	0.116	0.028	0.072
		A	6.206	6.324	6.203	0.118	0.003	0.060
	C5	G	5.783	5.796	5.718	0.013	0.065	0.039
		A	5.767	5.784	5.736	0.017	0.031	0.024
	C6	G	6.026	6.168	5.982	0.142	0.044	0.093
		A	6.006	6.168	5.964	0.162	0.042	0.102
	O32	G	8.766	8.779	8.720	0.013	0.046	0.029
		A	8.786	8.795	8.760	0.009	0.026	0.017
	S34	G	16.235	16.425	15.793	0.190	0.442	0.316
		A	16.342	16.531	15.591	0.189	0.751	0.470

4. CONCLUSION

Using the DFT/B3LYP method with the 6-31G**, the molecular geometry and molecular reactivity of four pyridazine derivatives were investigated leading to the following conclusions:

1. All the studied quantum chemical descriptors are correlated with the experimental observations. Both experimental and theoretical calculations are in excellent agreement.
2. The adsorption will probably occur through the pyridazine ring in all the inhibitors.
3. The adsorption through the S atom in P1 and P4 is more pronounced than that through the O atom in P2 and P3, respectively.
4. The establishment of the hydrogen bond in P3 and P4 probably stabilize these molecules which reduce slightly their inhibition efficiencies.

ACKNOWLEDGEMENTS
We are grateful to the "Association Marocaine des Chimistes Théoriciens" (AMCT) for its help concerning the Gaussian 03 program.

References

1. X.J. Raj, N. Rajendran, *Int. J. Electrochem. Sci.*, 6 (2011) 348.
2. B.E. Amitha Rani, Bharathi Bai J. Basu, *Int. J. Corros.*, 1 (2012) 1.
3. R.M. Issa, M.K. Awad, F.M. Atlam, *Appl. Surf. Sci*., 255 (2008) 2433.
4. B. Zerga, A. Attayibat, M. Sfaira, M. Taleb, B. Hammouti, M. Ebn Touhami, S. Radi, Z. Rais, *J. Appl. Electrochem*., 40 (2010) 1575.
5. M.B. Cisse, B. Zerga, F. El Kalai, M. Ebn Touhami, M. Sfaira, M. Taleb, B. Hammouti, N. Benchat, S. El kadiri, A.T. Benjelloun, *Surf. Rev. Lett.*, 18 (2011) 303.
6. S. Aloui, I. Forsal, M. Sfaira, M. Ebn Touhami, M. Taleb, M.F. Baba, M. Daoudi, *Portugaliae Electrochim. Acta*, 27 (2009) 599.
7. M. Bouklah, N. Benchat, A. Aouniti, B. Hammouti, M. Benkaddour, M. Lagrenée, H. Vezin, F. Bentiss, *Prog. Org. Coat*., 51 (2004) 118.
8. A. Chetouani, A. Aouniti, B. Hammouti, N. Benchat, T. Benhadda, S. Kertit, *Corros. Sci.*, 45 (2003) 1675.
9. M. Bouklah, N. Benchat, B. Hammouti, A. Aouniti, S. Kertit, *Mat. Lett.*, 60 (2006) 1901.
10. A. Chetouani, B. Hammouti, A. Aouniti, N. Benchat, T. Benhadda, *Prog. Org. Coat*., 45 (2002) 373.
11. B. Zerga, R. Saddik, B. Hammouti, M. Taleb, M. Sfaira, M. Ebn Touhami, S.S. Al-Deyab, N. Benchat. *Int. J. Electrochem. Sci*., 7 (2012) 631.
12. B. Zerga, B. Hammouti, M. Ebn Touhami, R. Touir, M. Taleb, M. Sfaira, M. Bennajeh, I. Forssal. *Int. J. Electrochem. Sci*., 7 (2012) 471.
13. Gaussian 03, Revision B.01, M.J. Frisch, G.W. Trucks, H.B. Schlegel, G.E. Scuseria, M.A. Robb, J.R. Cheeseman, J.A. Montgomery Jr., T. Vreven, K.N. Kudin, J.C. Burant, J.M. Millam, S.S. Iyengar, J. Tomasi, V. Barone, B. Mennucci, M. Cossi, G. Scalmani, N. Rega, G.A. Petersson, H. Nakatsuji, M. Hada, M. Ehara, K. Toyota, R. Fukuda, J. Hasegawa, M. Ishida, T. Nakajima, Y. Honda, O. Kitao, H. Nakai, M. Klene, X. Li, J.E. Knox, H.P. Hratchian, J.B. Cross, C. Adamo, J. Jaramillo, R. Gomperts, R.E. Stratmann, O. Yazyev, A.J. Austin, R. Cammi, C. Pomelli, J.W. Ochterski, P.Y. Ayala, K. Morokuma, G.A. Voth, P. Salvador, J.J. Dannenberg, V.G. Zakrzewski, S. Dapprich, A.D. Daniels, M.C. Strain, O. Farkas, D.K. Malick, A.D. Rabuck, K. Raghavachari, J.B. Foresman, J.V. Ortiz, Q. Cui, A.G. Baboul, S. Clifford, J. Cioslowski, B.B. Stefanov, G. Liu, A. Liashenko, P. Piskorz, I. Komaromi, R.L. Martin, D.J. Fox, T. Keith, M.A. Al-Laham, C.Y. Peng, A. Nanayakkara, M. Challacombe, P.M.W. Gill, B. Johnson, W. Chen, M.W. Wong, C. Gonzalez, and J.A. Pople, *Gaussian, Inc., Pittsburgh PA*, 2003.
14. A.D. Becke, *Chem. Phys.*, 98 (1993) 5648.
15. A.D. Becke, *Phys. Rev. A.*, 38 (1988) 3098.
16. C. Lee, W. Yang, R.G. Parr, *Phys. Rev. B.*, 37 (1988) 785.
17. C.C. Zhan, J. A. Nichols, D.A. Dixon, *J. Phys. Chem. A*, 107 (2003) 4184.
18. N.O. Obi-Egbedi , I.B. Obot, *Corros. Sci.*, 53 (2011) 263.
19. P. Udhayakala , T.V. Rajendiran, *JCBPSC,* 2 (2012) 172.
20. P. Udhayakala, A. Jayanthi, T.V. Rajendiran, *Der Pharma Chemica*, 3 (2011) 528.
21. W. Wang, W.J. Mortier, *J. Am. Chem. Soc*., 108 (1986) 5708.
22. K.F. Khaled, *Electrochim. Acta,* 22 (2010) 6523.
23. V.S. Sastri, J.R. Perumareddi, *Corrosion,* 53 (1997) 617.
24. A.E. Reed, L.A. Curtiss, F. Weinhold, *Chem. Rev,* 88 (1988) 899.

25. N.O. Eddy, S.R. Stoyanov, E.E. Ebenso, *Int. J. Electrochem. Sci.*, 5 (2010) 1127.
26. N.O. Obi-Egbedi, I.B. Obot, M. I. El-Khaiary, S. A. Umoren, E. E. Ebenso, *Int. J. Electrochem. Sci.*, 6 (2011) 5649.
27. G. Gece, S. Bilgiç, *Corros. Sci.*, 8 (2009) 1876.
28. E.E. Ebenso, D.A. Isabiry, *Int. J. Mol. Sci.*, 11 *(*2010) 2473.
29. I. Lukovits, E. Kalman, F. Zucchi, *Corrosion*, 57 (2001) 3.
30. M.A. Quijano, M.P. Pardav, A. Cuán, M.R. Romo, G.N. Silva, R.Á. Bustamante, A.R. López, H.H. Hernández, *Int. J. Electrochem. Sci.*, 6 (2011) 3729.